JOURNAL OF Applied Polymer SCIENCE

Synthesis and characterization of fluorinated organic–inorganic hybrid coatings on tinplate

Yongqin Fang, Di Wang, Xin Jing, Bosong Xue
Design and Research Institute, ChangZhou University, Changzhou 213164, China
Correspondence to: Y. Fang (E-mail: f13506119729@126.com)

ABSTRACT: Fluorinated organic–inorganic hybrid coatings with interpenetrating network for corrosion protection of tinplate were prepared by hydrolysis and condensation reaction of tetraethoxysilane and 3-methacryloxypropyltrimethoxysilane, followed by radical polymerization of trimethylolpropane triacrylate dodecafluoroheptyl methacrylate. The highly crosslinked organic network was developed and attached to the inorganic moieties through covalent Si–C bonds. The hybrid coatings were characterized by scanning electron microscope, water contact angle, Fourier transformed infrared spectroscopy, and thermogravimetric analysis. Their anticorrosion performances were evaluated by potentiodynamic polarization, electrochemical impedance spectroscopy and salt spray test. The results indicated that the fluorinated hybrid coatings exhibited excellent anticorrosion ability by forming a hydrophobic physical barrier between tinplate substrate and its external environment. © 2015 Wiley Periodicals, Inc. J. Appl. Polym. Sci. **2015**, *132*, 42428.

KEYWORDS: coatings; crosslinking; electrochemistry; radical polymerization; surfaces and interfaces

Received 31 January 2015; accepted 30 April 2015
DOI: 10.1002/app.42428

INTRODUCTION

Tinplate has become an important material because of its excellent properties.[1,2] As a result, it has been wide-ranging used in the food packaging field. However, tinplate is prone to be corroded when exposed to corrosion environment. Then, tinplate would lose its shiny appearance and excellent properties.[3] Thus, corrosion protection of tinplate is needed.

In recent years, silica sol–gel coatings are considered to be a promising corrosion protection material for different metal substrates, due to its outstanding adhesion,[4,5] anticorrosion ability,[6–12] scratch resistance,[13–15] and various surface wettabilities[16,17] on the coated substrates.

Sarmento *et al.*[17] have studied the polysiloxane hybrid films based on tetraethoxysilane (TEOS), 3-methacryloxypropyltrimethoxysilane (MPTS), and methyl methacrylate (MMA) on stainless tinplate substrates, exhibiting better corrosion protection for the stainless steel samples. However, the barrier effect of the hybrid coatings is not very well due to the low crosslinking density of the silane molecules. Xiu *et al.*[18] have illustrated the incorporation of silica nanoparticles into a hybrid organic–inorganic sol–gel coating, which was constructed from TEOS, MPTS. It was found that a better corrosion protection and super-hydrophobicity properties for the coated tinplate substrates compared to uncoated ones. However, some drawbacks exist in sol–gel coatings.[19] During the drying process, capillary forces and solvent evaporation stresses result in cracks and pores which destroy the physical barrier and will affect the performance of the coatings in corrosion protection. To maintain the integrity of films, the incorporation of organic monomer into sol–gel films has been extensively investigated.[20–22] Among the organic components, fluorinated polymers are particularly appealing candidates in terms of their high hydrophobic properties originating from fluorine as well as good adhesion between the hybrid coatings and substrates.

In this work, the hybrid coatings were synthesized by the acid-catalyzed hydrolytic co-polycondensation of TEOS and MPTS, followed by radical polymerization with trimethylolpropane triacrylate (TMPTMA) and dodecafluoroheptyl methacrylate (DFMA). The tri-functional monomer, TMPTMA, with three C=C double bonds, was used to develop a higher degree crosslinking between organic and inorganic networks through covalent Si–C bonds. In addition, the fluorinated acrylate, DFMA, with low surface free energy was used to improve the hydrophobic properties of the film. The hybrid coatings were characterized by scanning electron microscope (SEM), Fourier transformed infrared spectroscopy (FTIR), water contact angle (WCA), and thermogravimetric analysis (TGA). The corrosion resistance performances of the hybrid coatings deposited on tinplate were evaluated by potentiodynamic scan (PDS), electrochemical impedance spectroscopy (EIS), and salt spray test (SST).

EXPERIMENTAL

Materials

All chemicals used were commercially available. MPTS (Aldrich, 98%) and TEOS (Aldrich, 98%) were used as received. TMPTMA (98%) was obtained from Acros Organics. DFMA (95%) was purchased from XeoGia Fluorine-Silicon Chemical (China). Benzoyl peroxide (BPO, Reagen, 98%) was used as the initiator, and it was re-crystallized in ethanol solution before use. Absolute ethanol, acetone, nitric acid was purchased from Aladdin Company (Shanghai, China). Deionized water was used through the experiments.

Preparation of the Hybrid Coatings

The hybrid coatings were prepared by the sol–gel method in two successive steps: In the first step, the hydrolysis/polycondensation reaction involving the silicon alkoxide was performed by catalysis with HNO_3 at a pH value between 3 and 4 in absolute ethanol. Upon adding the deionized water for 1 h, the solution was under constant stirring for 3 h at room temperature. In the second step, the sol was diluted with absolute ethanol, and the temperature was increased to 70°C. Subsequently, TMPTMA, DFMA, and BPO were added to the closed flask within 1.5 h. As a consequence, a free radical polymerization of C=C occurred through a thermal decomposition of BPO at 70°C for about 8 h in a thermostatic water bath. The polymerization was carried out under a nitrogen atmosphere. As last, the homogenous and transparent hybrid sol was obtained.

The hybrid coatings prepared at the following MPTS/TMPTMA/DFMA molar ratio of 1 : 0.4 : 0.125, 1 : 0.4 : 0.25, 1 : 0.4 : 0.375, and 1 : 0.4 : 0.5 were denoted as F1, F2, F3, and F4, respectively, and the unmodified sample was marked as Sol. The molar ratio of BPO to C=C groups was controlled at 0.01. The other optimized molar ratios were kept constant: MPTS/TEOS = 1.0, ethanol/Si = 4.0, H_2O/Si = 3.0.

The procedure and the chemical structure of the hybrid coating at various steps are described in Figure 1.

As shown in Figure 1, the hybrid coatings have been produced by a sol–gel process consisting of two successive stages. The first step is the formation of the linear sol with methacryloxy functional groups by hydrolysis and condensation of MPTS and TEOS [see Figure 1(a)]. In the second step, the methacryloxy functional sol, DFMA, and TMPTMA with three C=C double bonds are crosslinked through a radical polymerization reaction and the hybrid coatings with interpenetrating network were obtained [see Figure 1(b)]. Aging would result in further condensation reaction and the formation of Si-O-Si three-dimensional network, which would improve the corrosion resistance of the hybrid coatings on tinplate. Silanols (Si–OH) is adsorbed onto the metal surface spontaneously through strong van der Waals bonds between the polymer molecules and the metallic surface, forming stable covalent Fe–O–Si bonds during the heat-treatment process [see Figure 1(c)].[23]

Surface Preparations and Coating Method

Tinplates (150 × 70 × 3 mm^3) were used as substrates, which were polished by metallography sand paper, up to a grade #800. After degreased with acetone and cleaned with distilled water, the tinplate was dried at 60°C for 2 h. The substrates were then dipped in the sol and withdrawn at a rate of 14 cm/min. Then the coated samples were dried at low temperature (60°C) for 5 h. Finally, the hybrid coatings were cured in an oven at a temperature of 110°C (heating rate 1°C/min) for 3 h.

Characterization

The surface morphologies of Sol, F1, F2, F3, and F4 coated on tinplates were characterized by SEM (SUPRA55, ZEISS, Germany), the images were taken using a field-emission SEM operated at an accelerating voltage of 5 kV. An energy dispersive X-ray spectroscopy (EDS) system in the same tool was used to determine the chemical composition of same at an applied voltage of 5 kV.

WCA analysis was measured to evaluate the hydrophobic properties of the hybrid coatings using DSA 100 (KRÜSS, Germany) with sessile drop method. In order to avoid any surface contamination, all specimens were washed with acetone, ethanol, and deionized water in sequence and accurately dried just before measurement. A 3-μL drop of distilled water was put on the surface with a microliter syringe and observed through an optical microscope. More than five contact angles on the different site of the film were averaged to get a reliable value for each sample.

Fourier transform infrared (FTIR) spectroscopy was recorded using a Nicolet Protégé 460 spectrometer (Thermo Fisher) in the wavenumber range of 400–4000 cm^{-1} with a resolution of 4 cm^{-1} and accumulation of 32 scans. The hybrid coatings were vacuum dried at 110°C for 2 h and subsequently grinded into powder and then mixed with KBr to press into tablets for FTIR measurements.

To evaluate the thermal behavior of the hybrid coatings, TGA were performed on TG 209 F1 (NETZSCH, Germany). About 5 mg samples of the hybrid coatings were placed into the platinum crucibles in nitrogen atmosphere from ambient temperature to 650°C with a constant heating rate of 10°C/min.

Both the PDS and EIS studies were carried out using a workstation (PGSTAT 302, Autolab, Switzerland) at room temperature in a 3.5 wt % NaCl solution. There were three components electrochemical cells consisting of the samples as working electrode, platinum sheet as the counter electrode and saturated calomel electrode (SCE) as a reference electrode. Potentiodynamic tests were conducted at a scan rate of 0.01 V/s after 2 h immersion in the electrolyte. EIS was recorded in a frequency range from 10^{-2} to 10^5 Hz with perturbation amplitude of 10 mV at the corrosion potential.

SST was performed according to GB/T 1771–2007. A solution of 5 wt % NaCl water was continuously sprayed in a closed testing chamber at 35°C and 0.1 MPa.

RESULTS AND DISCUSSION

Scanning Electron Microscopy Analysis

SEM micrographs of the sols and the fluorinated organic–inorganic hybrid films are shown in Figure 2. It clearly shows a strong effect of the amount of DFMA on the surface morphology of the hybrid films. Figure 2(a) shows that the sol film

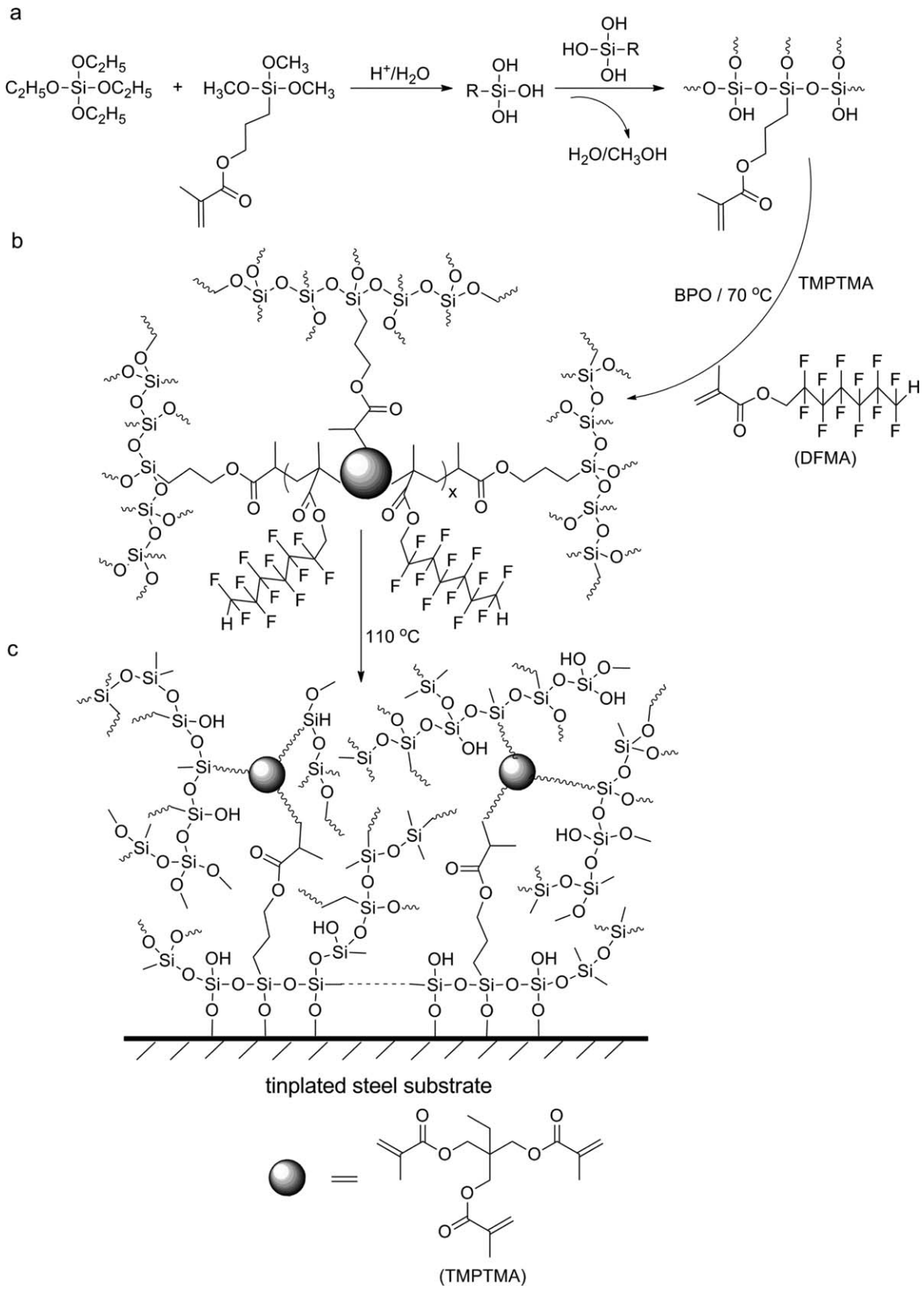

Figure 1. Reaction scheme of the formation of hybrid coatings: (a) hydrolysis and condensation of TEOS and MPTS; (b) crosslinking reaction; (c) the bonding mechanism between silane molecules and metal substrate.

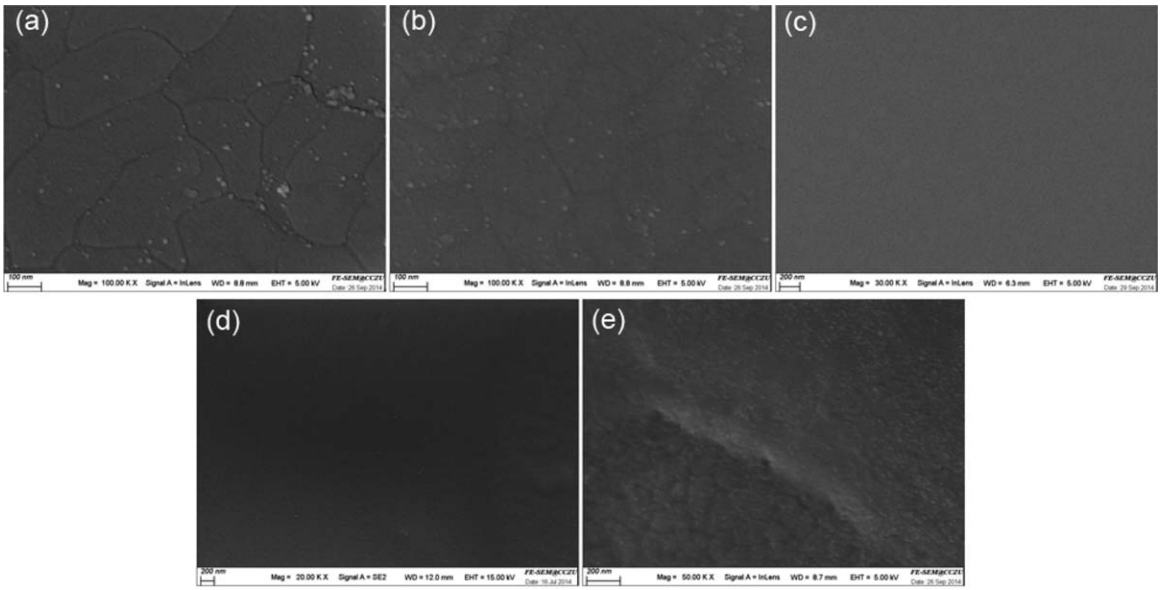

Figure 2. Surface morphologies of the hybrid coatings covered tinplate substrate (a) sol, (b) F1, (c) F2, (d) F3, and (e) F4.

tends to exhibit brittleness and microcracks. These cracks are presumably formed during the dry process as the result of strong capillary forces, owing to the different expansion coefficient between the sol–gel-derived films and the metallic substrates. As illustrated in Figure 2(b–d) that the fluorinated hybrid films have a smooth homogeneous, and highly adherent protective surface without detectable cracks. There results can be attributed to the increase of the flexible organic compositions, which could relax the stress and reduce the defects caused by the volume shrinkage of silicon network. However, F4 film tends to exhibit nonuniform thickness and shrinks, because the higher DFMA content increase the surface tension and the film-forming was bad.

In order to analyze the chemical composition of the hybrid film, the film was examined by EDS and the result is shown in Figure 3. The spectrum shows the presence of Si, O, F, and C. It is clear that DFMA was copolymerized with the MPTS/TEOS sol in the free radical polymerization process.

Contact Angle Analysis

WCA is commonly used as a criterion for the evaluation of hydrophobicity of a solid surface.[24] WCA (θ) usually describes

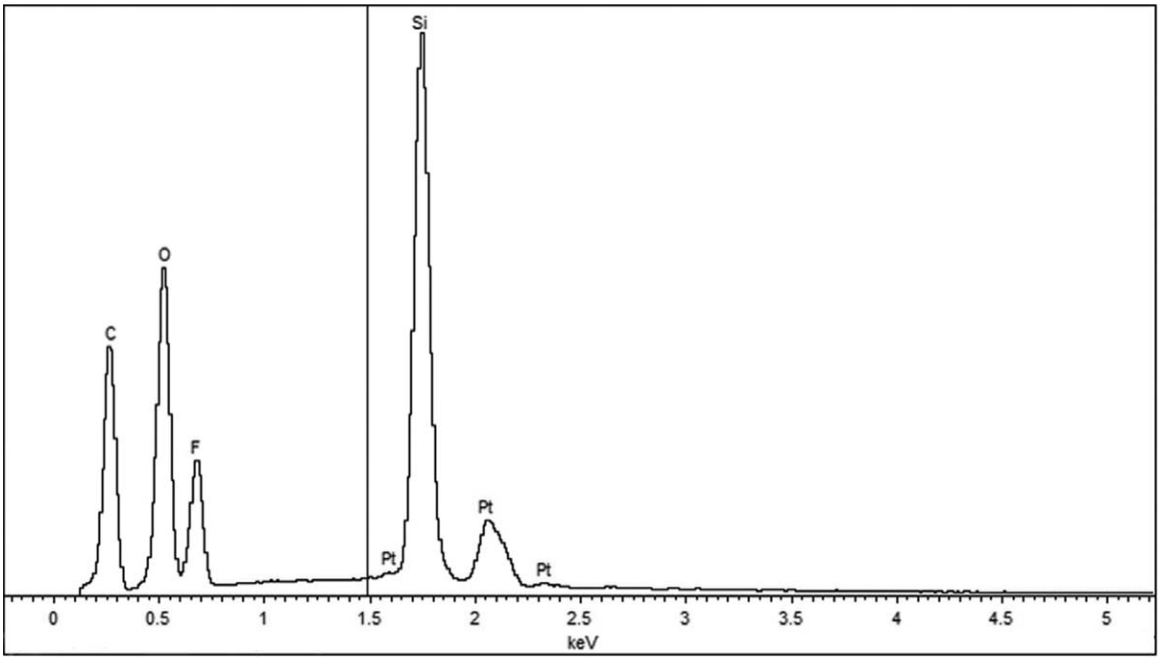

Figure 3. EDS spectrum of the fluorinated hybrid coating.

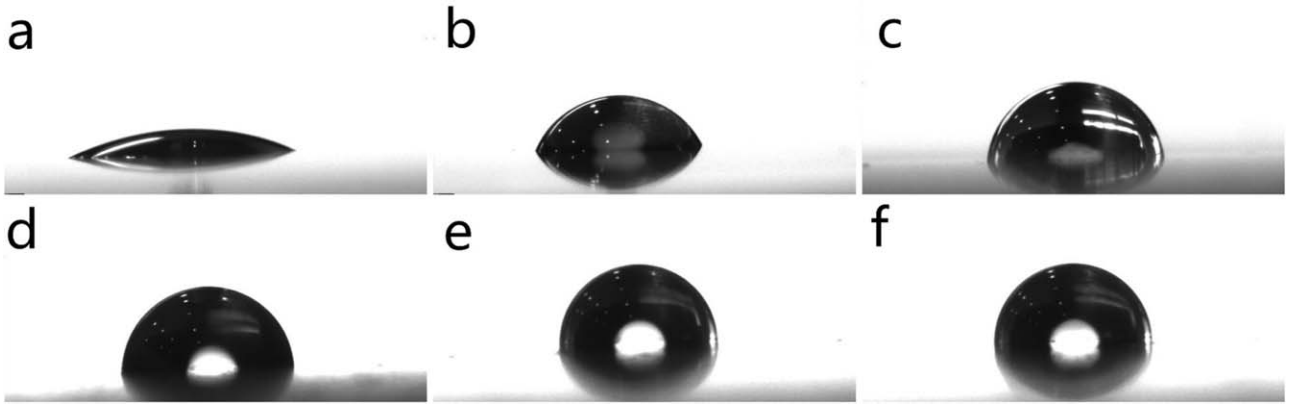

Figure 4. Photos of water droplet on tinplate surfaces: (a) bare steel, (b) Sol, (c) F1, (d) F2, (e) F3, and (f) F4.

the hydrophobic behavior of surface. The surface is hydrophobic when θ is higher than 90° and the surface is hydrophilic when θ is lower than 90°.[25] To reduce the surface free energy of the films, fluorine-contained monomers were used to copolymerize with the sols. Figure 4 shows the images of water droplet on the tinplate surfaces. WCA is 25° on the bare steel surface. The contact angles of sol coating is 61°, while in the cases of F1–F4 are 83°, 87°, 93°, 96°, respectively. The results showed that nonfluorine-contained films had evident hydrophilicity. However, when a little amount of fluorinated monomer was added into copolymerization, which greatly increasing the WCA of the surfaces of the coatings. It was shown that -CF_3 groups on the surface would give lower surface energy of the films. Furthermore, the more fluorine atoms contained in the fluorinated monomers, the greater WCA of their copolymer films were. It is obvious that the increasing of WCA may be attributed to migration and enrichment of more fluorinated groups located on the film surface, which is consistent with those reported in the literatures.[26]

FTIR Analysis

FTIR spectra of the hybrid films are shown in Figure 5. The absorption band at 3454 cm^{-1} corresponds to the O-H stretching vibration of both water and silanol groups;[12] 1733 cm^{-1} is stretching vibration peak of C=O. The strong and broad peaks in the 1200–1050 cm^{-1} region, together with a band at 795 cm^{-1}, corresponding to the vibration absorption of Si-O-Si groups originating from TEOS and MPTS,[27,28] indicate the formation of the Si-O-Si bearing three-dimensional network. The Sol and fluorinated hybrid coatings have similar characteristic peaks in the range of 4000 to 400 cm^{-1}. The asymmetric stretching, symmetric stretching, scissoring and stretching modes of C-H of MPTS, DFMA, and TMPTMA are evident at around 2970, 2896, 1473, and 1391 cm^{-1}, respectively. The decreased in the C=C bond absorption (1638 cm^{-1}) show the reaction of TMPTMA with MPTS and DFMA in the free radical polymerization process.

Spectrum (b) shows new peaks of C-F stretching vibration at 1303 cm^{-1} and wagging vibration at 691 cm^{-1}.[29,30] However, the stretching vibration of -CF_2 and -CF_3 groups at about 1247–1174 cm^{-1}, were overlapped with the corresponding band of Si-O-Si.[31] Therefore, FTIR spectra confirmed that DFMA had had taken part in the copolymerization and resulted in formation of the interpenetrating network of hybrid coatings.

Thermal Analysis

The thermal stability of the hybrid coatings were examined by TGA curves and the differential weight loss (DTG) of the powder samples, as illustrated in Figure 6. The sol samples initially begin to degrade in the first stage at approximately 100°C due to the loss of nonbonded water. Further increase in temperature up to 398°C caused the degradation of organic moieties present in the TEOS/MPTS.[32] When the temperature increase to above 500°C, the degradation can be attributed to the dehydration of silanol groups in the SiO_2 network.[33] It should be noted that the hybrid coatings (F1, F2, F3, F4) show higher thermal stability of about 427, 430, 431, and 432°C, respectively, compared with unmodified coating. Obviously, the thermal stability of the films was improved by the addition of TMPTMA and DFMA. This phenomenon can be attributed to two aspects. On the one hand, the addition of TMPTMA can lead to a higher crosslinking network. On the other hand, the C-F bond with high bond energy was able to shield and protect the nonfluorinated segment.[34]

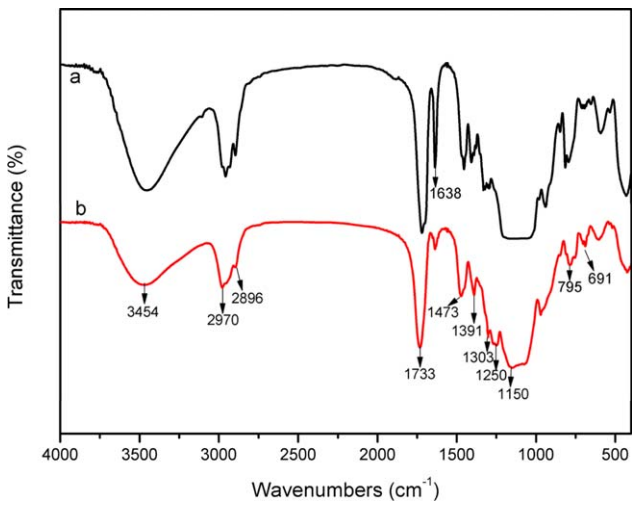

Figure 5. FTIR spectrum of (a) sol coating and (b) fluorinated hybrid coating. [Color figure can be viewed in the online issue, which is available at wileyonlinelibrary.com.]

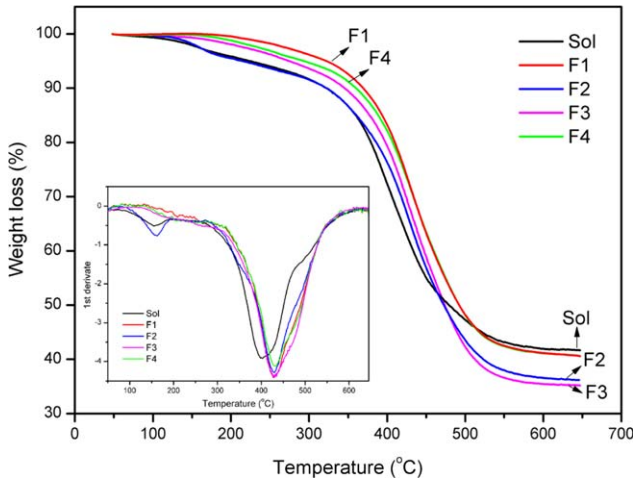

Figure 6. TGA and DTG (insert) curves of the sol and fluorinated hybrid coatings. [Color figure can be viewed in the online issue, which is available at wileyonlinelibrary.com.]

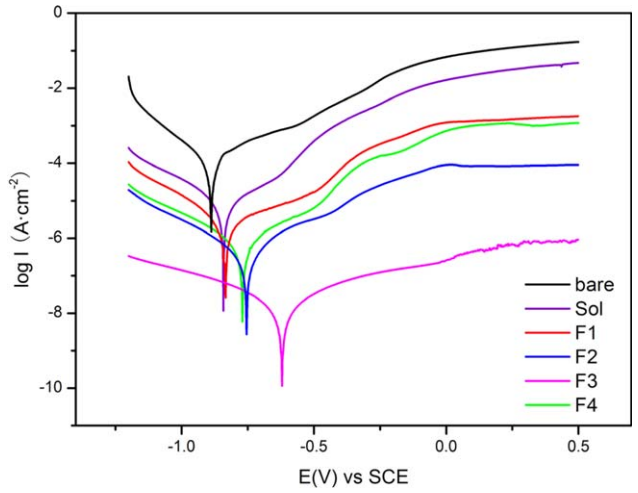

Figure 7. Polarization curves of bare steel, sol, and fluorinated hybrid coatings in 3.5 wt % NaCl solution. [Color figure can be viewed in the online issue, which is available at wileyonlinelibrary.com.]

Corrosion Analysis

Polarization Curves. The polarization curves were recorded for bare electrode and coated electrodes with different amounts of DFMA after 2 h of immersion in neutral 3.5 wt % NaCl solution. They are shown in Figure 8. Corresponding corrosion parameters are listed in Table I. These parameters are obtained via extrapolation of the anodic region of the Tafel curve.[35] The value of the coating anticorrosion efficiencies (η) is calculated by the following equation:[36]

$$\eta = \left(1 - \frac{\text{icorr}}{\text{i°corr}}\right) \times 100\% \quad (1)$$

where $i°_{corr}$ and i_{corr} are the corrosion current density of bare and coated electrodes, respectively.

According to the polarization curve (Figure 7) and the related corrosion parameters (Table I), when compared to the bare sample, the coated samples have a positive shift in the E_{corr} value. In general, a good Tafel behavior is observed with the lower corrosion current density. According to Table I, when TMPTMA and DFMA were added to the hybrid coatings, the corrosion current density (I_{corr}) of sol, F1, F2, F3, and F4 samples are decreased, it is found to be significantly lower than that of bare sample. By comparing the value of the corrosion current density of the bare tinplate and coatings, the order is F3 > F2 > F4 > F1 > sol > bare. The values of the protection efficiency of Sol, F1, F2, F3, and F4 are calculated by eq. (1) to be 93.36, 98.18, 99.78, 99.99, and 99.52%, respectively. As compared to the bare tinplate (3.240×10^{-5} A cm^{-2}), the i_{corr} value for F3 hybrid coating (2.685×10^{-9} A cm^{-2}) is greatly reduced by four orders in magnitude. These results indicating that the incorporation of TMPTMA and DFMA at optimum concentrations increases the anticorrosion properties of the hybrid coatings due to higher crosslinked, dense and pore-free film has been formed. However, the films derived from the highest DFMA content (F4 sample) exhibited poor corrosion resistance. The deterioration of corrosion resistance ability will be mainly attributed to the present of nonuniform thickness and shrinks. The corrosive solutions were more easily attacked these defects and permeated into the coatings.

Electrochemical Impedance. EIS was used to evaluate the anticorrosion properties of the hybrid coatings. Figure 8 depicts the Bode plots for bare and coated electrodes with different amounts of DFMA after 2 h immersion in 3.5 wt % NaCl solution. According to the literature,[37] the value of impedance modulus (|Z|) is inversely proportional to the corrosion rate. The values of impedance modulus at 0.01 Hz ($|Z|_{0.01}$) are listed in Table I. As shown in Figure 8 and Table I, the |Z| values of

Table I. Electrochemical Parameters for the Bare Tinplate and Hybrid Coatings Covered Tinplate Electrodes Obtained from the Polarization Curves and EIS Measurements

				$\lvert Z\rvert_{0.01}$ (Ω cm^2)	
Electrode	E_{corr} (mv) (vs. SCE)	I_{corr} (A cm^{-2})	η (%)	4 h	168 h
Bare	888	3.240×10^{-5}	-	1.87×10^{3}	-
Sol	842	2.152×10^{-6}	93.36	1.81×10^{4}	2.05×10^{3}
F1	734	5.905×10^{-7}	98.18	1.21×10^{5}	7.31×10^{3}
F2	754	7.050×10^{-8}	99.78	6.59×10^{5}	3.37×10^{4}
F3	620	2.685×10^{-9}	99.99	3.42×10^{6}	6.59×10^{4}
F4	770	1.557×10^{-7}	99.52	3.05×10^{5}	2.12×10^{4}

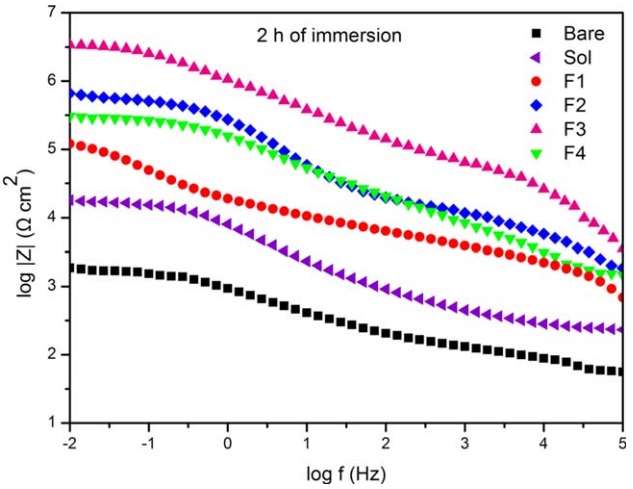

Figure 8. Bode plots representation of EIS results for bare steel and hybrid coatings covered steel electrodes after 2 h immersion in 3.5 wt % NaCl solution. [Color figure can be viewed in the online issue, which is available at wileyonlinelibrary.com.]

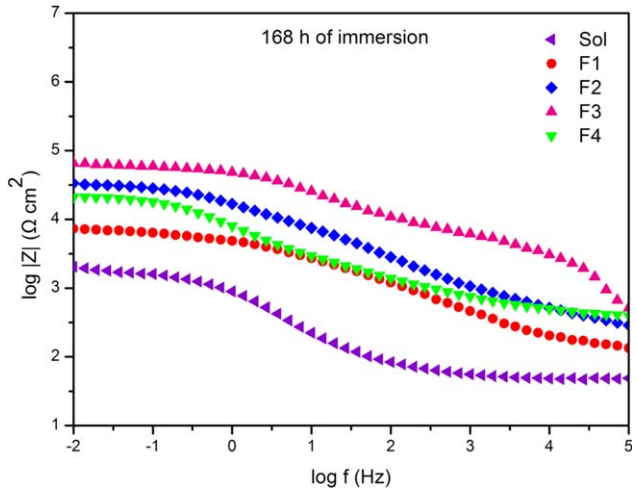

Figure 9. Bode plots representation of EIS results for Sol and fluorinated hybrid coatings covered tinplate electrodes after 168 h immersion in 3.5 wt % NaCl solution. [Color figure can be viewed in the online issue, which is available at wileyonlinelibrary.com.]

coated samples are higher than that of bare sample. This indicates that all the coated samples can provide a corrosion protection for tinplate. The $|Z|_{0.01}$ values for F3 (3.42×10^6 Ω cm^2) is greatly increased by three orders in magnitude compared to the bare steel (1.87×10^3 Ω cm^2). Sol coating reveals only a small increase, comparatively to the bare tinplate. Besides, the highest $|Z|_{0.01}$ value of coated samples shows that the F3 sample provides a better anticorrosion performance than F1, F2, and F4 samples. And the results of EIS match with the results of polarization curves.

Figure 9 shows Bode plots of EIS results for the coated samples after immersion of 168 h in 3.5 wt % NaCl solution and the $|Z|_{0.01}$ values are also listed in Table I. After 168 h of immersion, the impedance modulus of Sol sample with $|Z|_{0.01} = 2.05\times10^3$ Ω cm^2 is close to that of bare electrode, indicating that sol coating lose its anticorrosion ability. It can be found that the $|Z|_{0.01}$ value of F1 sample shifts to 7.31×10^3 and after 168 h of immersion. The result demonstrates that the F1 coating is also easy to be corroded, although its anticorrosion ability is better than pure sol coating. For F2 and F3 coatings, the $|Z|_{0.01}$ value decrease to 3.37×10^4 and 2.12×10^4 Ω cm^2 after 168 h of immersion, respectively. The results indicate that F2, F4 samples have better corrosion resistance. For F3 coating, the $|Z|_{0.01}$ value is 6.59×10^4 Ω cm^2 after 168 h of immersion, much higher than those for the bare sample. These results indicate the protective nature of fluorinated silane hybrid coatings and verify that F3 coating possesses relatively good anticorrosion ability.

Neutral Salt Spray Test. Figure 10 presents the results of the SSTs of the bare and coated tinplate after different exposure time. We can observe the bare tinplate was badly corroded after being exposed in salt spray for 48 h [see Figure 10(a)]. Figure 10(b) shows that large area of rust appears on the sol-coated tinplate surface after 120 h, confirming the limited corrosion protection capability of the unmodified sol–gel coating. Compared with the bare tinplate and sol coating, fluorinated modified coatings exhibited excellent anticorrosion properties.

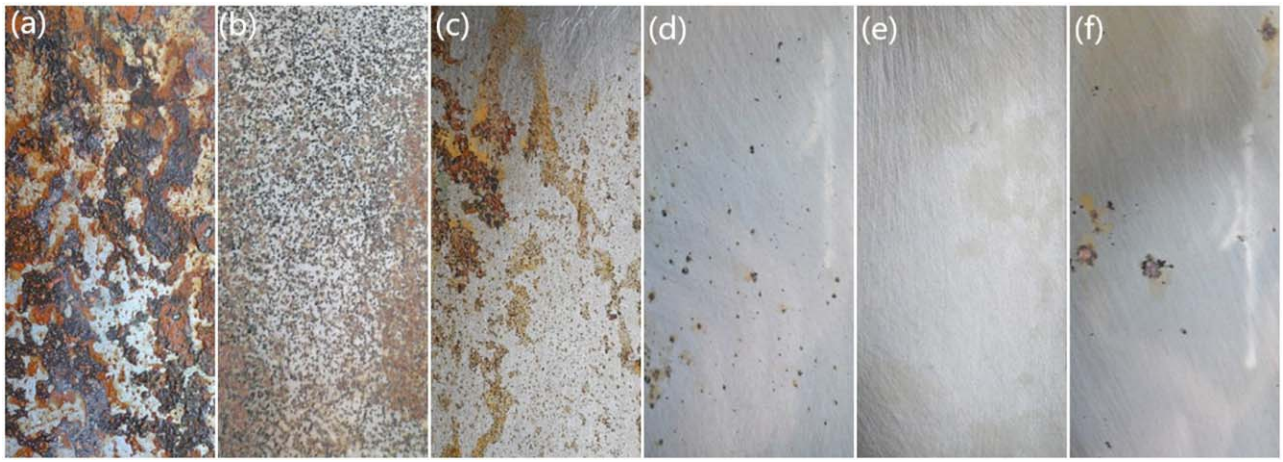

Figure 10. Photographs of sate spray test after different exposure times: (a) bare steel, (b) sol, (c) F1, (d) F2, (e) F3, and (f) F4. [Color figure can be viewed in the online issue, which is available at wileyonlinelibrary.com.]

Figure 10(c,d) shows that after 200 h, some corrosion has been found on F1 and F2 coatings, the progresses become more slowly than the bare and sol samples. Especially for F3, no obvious corrosion occurs on the tinplate surface after being exposed in salt spray for 240 h [see Figure 10(e)]. However, F4 undergoes mild damages with appearance of red corrosion product of tinplate after 200 h of exposure [see Figure 10(f)]. These favorable results suggest that the anticorrosion ability of sol coating can be enhanced by synergy of the crosslinking agent (TMPTMA) and the fluorinated organic monomer (DFMA). Those results of SST are in accordance with the results of electrochemical tests.

CONCLUSIONS

The effect of crosslinking agents (TMPTMA) and DFMA-modified hybrid coating was researched systematically. SEM measurements confirmed the formation of smooth, dense and homogenous film of the fluorinated hybrid coating on the surface of tinplate. Also the fluorinated hybrid coatings have a better thermal stability compared with the sol coating. The water repellent property of the fluorinated modified film acts as a physical barrier for water, oxygen, or other corrosive species from penetrating through the layer and reaching the substrate and thus preventing the oxidation of the tinplate surface. According to the results of electrochemical tests and SST, it reveals that the fluorinated organic–inorganic hybrid coatings exhibit advantageous barrier performance on tinplate due to the synergistic effect of crosslinked organic–inorganic structure and the water repellent property of the fluorinated organic monomer.

AUTHOR CONTRIBUTIONS

Conception and design: Yongqin Fang, Di Wang, Xin Jing. Acquisition, analysis and interpretation of data: Yongqin Fang, Di Wang, Xin Jing, Bosong Xue. Manuscript writing and revision: Yongqin Fang, Di Wang, Xin Jing, Bosong Xue. Final approval of manuscript: Yongqin Fang, Di Wang, Xin Jing.

REFERENCES

1. Ibrahim, M. A.; Abd El Rehim, S. S.; Hamza, M. M. *Mater. Chem. Phys.* **2009**, *115*, 80.
2. Lu, H. B.; Hu, Y.; Gu, M. H.; Tang, S. C.; Lu, H. M.; Meng, X. K. *Surf. Coat. Technol.* **2009**, *204*, 91.
3. Bhattacharyya, S.; Das, M. B.; Sarkar, S. *Eng. Fail. Anal.* **2008**, *15*, 711.
4. Atik, M.; de Lima Neto, P.; Avaca, L. A.; Aegerter, M. A. *Ceram. Int.* **1995**, *21*, 403.
5. Parkhill, R. L.; Knobbe, E. T.; Donley, M. S. *Prog. Org. Coat.* **2001**, *41*, 261.
6. Melanie, F.; Habiba, M.; Brice, G.; Jean-Philippe, B. *J. Non-Cryst. Solids* **2001**, *293*, 527.
7. Huang, K. Y.; Weng, C. J.; Lin, S. Y.; Yu, Y. H.; Yeh, J. M. *J. Appl. Polym. Sci.* **2009**, *112*, 1933.
8. Subasri, R.; Jyothirmayi, A.; Reddy, D. S. *Surf. Coat. Tech.* **2010**, *205*, 806.
9. Wolfgang, E. G.; Hansala, T.; Selma, H.; Matthias, P.; Andreas, K.; Gerhard, Z.; Gerhard, E. N. *Surf. Coat. Tech.* **2006**, *200*, 3056.
10. Peng, S.; Zhao, W.; Li, H.; Zeng, Z.; Xue, Q.; Wu, X. *Appl. Surf. Sci.* **2013**, *276*, 284.
11. Seifzadeh, D.; Golmoghani-Ebrahimi, E. *Surf. Coat. Tech.* **2012**, *210*, 103.
12. Liu, J. G.; Xu, L.; Fang, Y. Q. *J. Sol-Gel Sci. Technol.* **2014**, *71*, 246.
13. Malzbender, J.; With, G. *Surf. Coat. Tech.* **2001**, *135*, 202.
14. Nemeth, S.; Liu, Y. C. *Thin Solid Films* **2009**, *517*, 4888.
15. Brus, J.; Hlavatá, D.; Kamišová, H.; Matějka, L.; Strachota, A. *J. Appl. Polym. Sci.* **2004**, *92*, 937.
16. Zhao, Y.; Li, J.; Hu, J.; Shu, L.; Shi, X. *J. Disper. Sci. Technol.* **2011**, *32*, 969.
17. Sarmento, V. H. V.; Schiavetto, M. G.; Hammer, P.; Benedetti, A. V.; Fugivara, C. S.; Suegama, P. H.; Pulcinelli, S. H.; Santilli, C. V. *Surf. Coat. Tech.* **2010**, *204*, 2689.
18. Wen, X. F.; Wang, K.; Pi, P. H.; Yang, J. X.; Cai, Z. Q.; Zhang, L. J.; Qian, Y.; Yang, Z. R.; Zheng, D. F.; Cheng, J. *Appl. Surf. Sci.* **2011**, *258*, 991.
19. Zheludkevich, M. L.; Salvado, I. M.; Ferreira, M. G. S. *J. Mater. Chem.* **2005**, *15*, 5099.
20. Voevodin, N. N.; Grebasch, N. T.; Soto, W. S.; Arnold, F. E.; Donley, M. S. *Surf. Coat. Tech.* **2001**, *140*, 24.
21. Khramov, A. N.; Voevodin, N. N.; Balbyshev, V. N.; Mantz, R. A. *Thin Solid Films* **2005**,*483*, 191.
22. Quinet, M.; Neveu, B.; Moutarlier, V.; Audebert, P.; Ricq, L. *Prog. Org. Coat.* **2007**, *58*, 46.
23. Kirtay, S. *Prog. Org. Coat.* **2014**, *77*, 1861.
24. Zhao, F.; Zeng, X.; Li, H.; Zhang, J. *Colloid Surf. A* **2012**, *396*, 328.
25. Zhang, B. T.; Liu, B. L.; Deng, X. B.; Cao, S. S.; Hou, X. H.; Chen, H. L. *Appl. Surf. Sci.* **2007**, *254*, 452.
26. Wang, J.; Zeng, X. R.; Li, H. Q. *J. Coat. Technol. Res.* **2010**, *7*, 469.
27. Kang, S.; Hong, S. I.; Choe, C. R.; Park, M.; Rim, S.; Kim, J. *Polymer* **2001**, *42*, 879.
28. Yu, Q.; Xu, J.; Han, Y. *Appl. Surf. Sci.* **2011**, *258*, 1412.
29. Cui, X. J.; Zhong, S. L.; Yan, J.; Wang, C. L.; Zhang, H. T.; Wang, H. Y. *Colloid. Surface. A* **2010**, *360*, 41.
30. Cheng, X. L.; Chen, Z. X.; Shi, T. S.; Wang, H. Y. *Colloid. Surface. A* **2007**, *292*, 119.
31. Li, K.; Zeng, X.; Li, H. *Appl. Surf. Sci.* **2014**, *298*, 214.
32. Nagappan, S.; Choi, M. C.; Sung, G. *Macromol. Res.* **2013**, *21*, 669.
33. Hammer, P.; dos Santos, F. C.; Cerrutti, B. M.; Pulcinelli, S. H.; Santilli, C. V. *J. Sol-Gel Sci. Technol.* **2012**, *63*, 266.
34. Bai, R.; Qiu, T.; Duan, M. *Colloid Surf. A* **2012**, *396*, 251.
35. Rath, P. C.; Besra, L.; Singh, B. P.; Bhattacharjee, S. *Ceram. Int.* **2012**, *38*, 3209.
36. Le, D. P.; Yoo, Y. H.; Kim, J. G.; Cho, S. M.; Son, Y. K. *Corros. Sci.* **2009**, *51*, 330.
37. CatalÁ, R.; CabaÑEs, J. M.; Bastidas, J. M. *Corros. Sci.* **1998**, *40*, 1455.